Superfluidity of Mesoscopic Bose Gases under Varying Confinements

Kwangsik Nho[1] and D. Blume[1]

[1]Department of Physics and Astronomy, Washington State University, Pullman, Washington 99164-2814, USA

(Received 7 June 2005; published 31 October 2005)

The superfluid fraction N_s/N of 27 bosons under varying confinement is investigated at finite temperature using well-known properties of the harmonic oscillator and the microscopic path integral Monte Carlo method. We find that N_s/N (i) is essentially independent of the interaction strength for all temperatures considered, (ii) changes profoundly as the effective dimensionality is varied from three to one dimensional, (iii) is approximately equal to the condensate fraction N_0/N for spherical Bose gases, and (iv) deviates dramatically from N_0/N for highly elongated Bose gases.

DOI: 10.1103/PhysRevLett.95.193601 PACS numbers: 03.75.Hh, 67.40.Kh

Macroscopic objects such as liquid ^{4}He show many peculiar properties that can be attributed to superfluidity [1]. Among these are the absence of viscosity, the occurence of persistent currents, the existence of vortices, and the reduction of the moment of inertia. Connections between manifestations of superfluidity and Bose Einstein condensation have been studied extensively in the context of liquid ^{4}He since the discovery of its superfluidity in 1938. While much progress has been made in our understanding of such strongly interacting systems, many questions remain unanswered.

Although strictly speaking the transition temperature of a Bose gas is defined only in the thermodynamic limit, its definition can be extended to finite systems (see, e.g., Refs. [2,3]). Phase transitions are, however, ''smeared out'' for finite systems. Thanks to the realization of gaseous Bose Einstein condensates (BECs), the study of superfluid effects of mesoscopic systems has become possible. Indeed, the creation of vortices [4,5] and vortex lattices [6] has been demonstrated in inhomogeneous Bose gases and, most recently, also in degenerate Fermi gases in the BEC-BCS crossover regime [7]. Following the work on ^{4}He enclosed in a cylinder [8], superfluidity of inhomogeneous systems can be described through their rotational properties. The superfluid fraction is defined by the departure of the quantum mechanical moment of inertia $\Theta_{\hat{n}}$ with respect to $\hat{n}$ from its classical, or rigid, value $\Theta_{\hat{n}}^{\mathrm{rig}}$. Here the moment of inertia $\Theta_{\hat{n}}$, $\Theta_{\hat{n}} = (\partial\langle\vec{L}\cdot\hat{n}\rangle_\omega/\partial\omega)_{\omega=0}$, is defined by the linear response of the system to a rotational field $H_{\mathrm{ext}} = -\vec{\omega}\cdot\vec{L}$, where $\vec{\omega} = \omega\hat{n}$; ω denotes the angular frequency and $\vec{L}$ the total angular momentum. The thermal expectation value $\langle\cdot\rangle_\omega$ is evaluated for the system perturbed by H_{ext}. The normal fraction is the part of the system that responds classically, i.e., $\Theta_{\hat{n}}/\Theta_{\hat{n}}^{\mathrm{rig}}$, and the superfluid fraction $(N_s/N)_{\hat{n}}$ is $1 - \Theta_{\hat{n}}/\Theta_{\hat{n}}^{\mathrm{rig}}$.

This Letter determines the temperature dependence of $\Theta_{\hat{n}}$ and $\Theta_{\hat{n}}^{\mathrm{rig}}$, and, hence, of the superfluid fraction, for small atomic gases with $N = 27$ bosons for varying confinement and interaction strength nonperturbatively using the essentially exact microscopic path integral Monte Carlo (PIMC) method [9]. For the ideal gas, we additionally determine thermal expectation values using well-known properties of the harmonic oscillator [10]. In contrast to ^{4}He clusters [11] or deformed nuclei [12], whose interaction strength and internal temperature are largely ''set by nature,'' atomic gases provide us with unprecedented control. The temperature can be controlled by changing the cooling scheme [13], the interaction strength can be tuned by applying an external magnetic field in the vicinity of a Feshbach resonance [14], and the dimensionality can be reduced by varying the external confinement [15]. Here we focus on the crossover from three-dimensional (3D) to one-dimensional (1D) behavior. We show that reduced dimensionality leads to an increase of the superfluid response. The superfluid fraction N_s/N for 3D gases roughly coincides with the condensate fraction N_0/N. In the quasi-1D regime, however, N_s/N is much larger than N_0/N. Our calculations show that the superfluid response depends, if at all, weakly on the strength of the atom-atom interactions.

Consider N bosons with mass m under external harmonic confinement,

$$H = \sum_{j=1}^{N}\left[\frac{-\hbar^2}{2m}\nabla_j^2 + \frac{1}{2}m(\omega_\rho^2\rho_j^2 + \omega_z^2 z_j^2)\right] + \sum_{j<k}^{N} V(r_{jk}). \quad (1)$$

Here ρ_j and z_j denote the transverse and longitudinal coordinate of the jth atom, respectively, and ω_ρ and ω_z the transverse and longitudinal angular frequency of the trapping potential, respectively. The atom-atom potential V depends on the interparticle distance r_{jk} between atom j and atom k. For the noninteracting gas, i.e., $V(r) = 0$, we calculate thermal expectation values in the grand canonical ensemble using well-known properties of the harmonic oscillator [10]. To simulate effectively repulsive Bose gases, we use a hard sphere potential $V(r)$ with 3D atom-atom scattering length a; in particular, $a = 0.004\,33$ and $0.0433a_z$, where $a_z = \sqrt{\hbar/(m\omega_z)}$. In this case, we use the numerically more involved PIMC technique [9], which

determines thermal expectation values in the canonical ensemble. For the purpose of the present study, differences between expectation values calculated in the grand canonical and in the canonical ensembles (see also Ref. [16]) are negligible.

To investigate the crossover from 3D to 1D for N bosons, we vary the angular frequency ω_ρ such that $L = 1$, 10, and 100, where $L = \omega_\rho/\omega_z$. The approximate 3D transition temperature T_c, obtained for vanishing atom-atom interactions, then depends on ω_ρ, ω_z, and N [the T_c used throughout this paper includes finite-size corrections; see, e.g., Eq. (19) in Ref. [17]]. A dotted line in Fig. 1 shows T_c as a function of the aspect ratio L for $N = 27$. Below, we report calculations for $L = 1$, 10, and 100 over a wide temperature range, i.e., $0.1 \lesssim T/T_c \lesssim 1.4$ (see vertical arrows in Fig. 1).

Highly elongated gases at $T = 0$ can, to a very good approximation, be described by an effective 1D Hamiltonian for any 3D scattering length a if $N/L \ll 1$ [18]. For $N = 27$ and $L = 100$, we find $N/L = 0.27$. At finite temperature, the behavior of highly elongated Bose gases depends on two energy scales, the oscillator energies $\hbar\omega_\rho$ and $\hbar\omega_z$ of the tight and weak confinement directions, respectively. For $N = 27$ and $L = 100$, three temperature regimes exist [2]: (i) T is larger than the 3D transition temperature T_c (excited transverse modes are occupied); (ii) T is lower than T_c but larger than the 1D transition temperature T_c^{1D} [3] (transverse excitations are largely frozen out); and (iii) T is smaller than T_c^{1D} (excited longitudinal modes are largely frozen out). For $N = 27$ and $L = 100$, the approximate 3D transition temperature is $k_B T_c = 36.0\hbar\omega_z$, while the approximate 1D transition temperature is $k_B T_c^{1D} = 6.77\hbar\omega_z$, corresponding to $0.19T_c$.

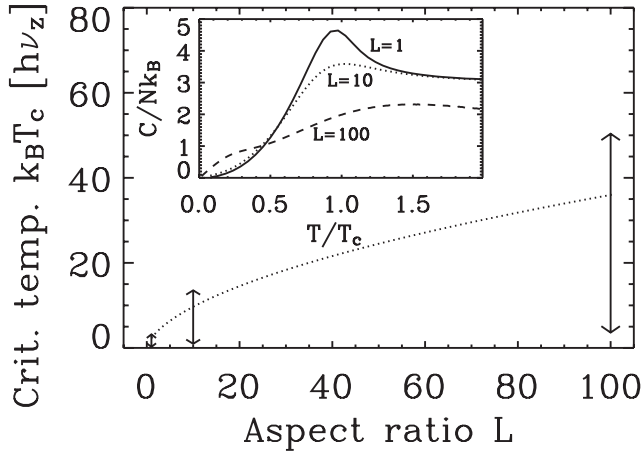

FIG. 1. Approximate 3D transition temperature $k_B T_c$ (see text) in units of $\hbar\omega_z$ ($\omega_z = 2\pi\nu_z$) as a function of L for $N = 27$. Vertical arrows indicate the interval $0.1 \leq T/T_c \leq 1.4$ for $L = 1$, 10, and 100. The inset shows the specific heat C divided by Nk_B calculated in the grand canonical ensemble as a function of T/T_c for $N = 27$ and varying L.

To understand the significance of the 3D transition temperature T_c, we calculate the specific heat C, $C = (\partial U/\partial T)_N$, where U denotes the internal energy [2], for the ideal gas in the grand canonical ensemble. The inset in Fig. 1 shows the specific heat C for $N = 27$ for three different aspect ratios, i.e., $L = 1$ (solid line), 10 (dotted line), and 100 (dashed line). Since the specific heat shows a peak, although broadened due to the finite size of the Bose gas, at $T/T_c \approx 1$ for $L = 1$ and 10 and at $T/T_c \approx 1.4$ for $L = 100$, it is justified to speak of a 3D transition temperature for Bose gases with as few as $N = 27$ atoms. In contrast, the transition to macroscopic occupation of the lowest energy state for the quasi-1D gas with $L = 100$, i.e., to "1D condensation," does not imprint a clear signature on the specific heat (see also Refs. [2,3]).

Figure 2 shows the expectation value of the absolute value of z (in the following denoted by $\langle|z|\rangle$) in units of a_z, calculated using the PIMC method, as a function of the scaled temperature T/T_c for (a) $L = 1$ and (b) $L = 100$ for three scattering lengths; $a = 0$ (diamonds), $a = 0.00433a_z$ (squares), and $a = 0.0433a_z$ (triangles). At low T/T_c, our expectation values of $|z|$ for $a = 0$ (circles) approach the zero-temperature value, i.e., $\langle|z|\rangle = 0.564a_z$. Since the energy of the transverse excitations increases with increas-

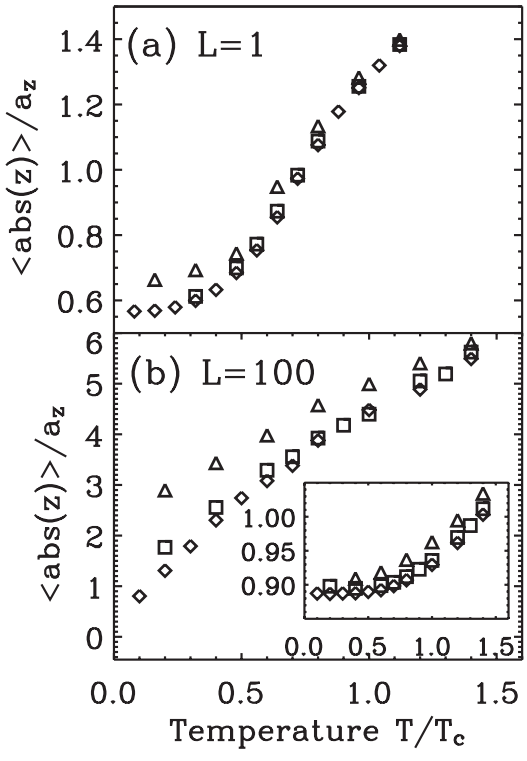

FIG. 2. PIMC expectation value of the absolute value of z in units of a_z as a function of T/T_c for $N = 27$ for (a) $L = 1$ and (b) 100. Diamonds show the results for $a/a_z = 0$, squares those for $a/a_z = 0.004\,33$, and triangles those for $a/a_z = 0.0433$. For $L = 100$, the inset shows the expectation value of ρ in units of a_ρ as a function of T/T_c. Statistical uncertainties are smaller than the symbol size [23].

ing L, the expectation value of $|z|$ for $L = 100$ approaches the zero-temperature value at a lower scaled temperature T/T_c than that for $L = 1$. For repulsive interactions, i.e., $a/a_z = 0.004\,33$ (squares) and $a/a_z = 0.0433$ (triangles), the expectation value of $|z|$ increases compared to that of the noninteracting gas.

The inset in Fig. 2(b) shows the expectation value of ρ in units of a_ρ, where $a_\rho = \sqrt{\hbar/(m\omega_\rho)}$, for $L = 100$ as a function of T/T_c (using the same symbols as in the main figure). At $T = 0$, the expectation value of ρ is $0.886a_\rho$ for the noninteracting gas. Just as the expectation value of $|z|$, that of ρ depends strongly on the interaction strength a. The nearly constant expectation value of ρ for $L = 100$ (for a given value of a) at low T/T_c indicates that the excitations in the transverse direction are frozen out for $T \lesssim 0.4T_c$ and, hence, for $T < T_c^{1D}$.

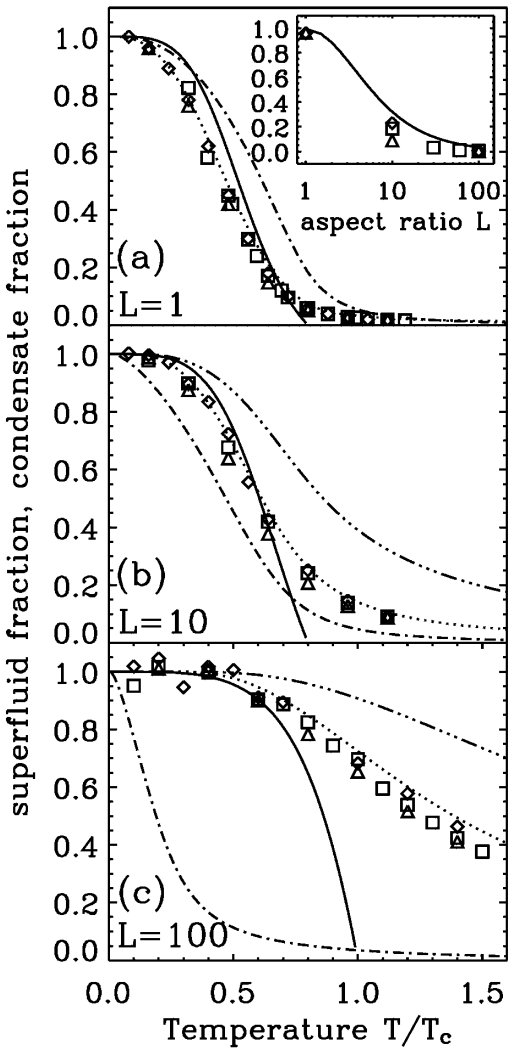

FIG. 3. Superfluid fraction $(N_s/N)_{\hat{z}}$ for $N = 27$ and (a) $L = 1$, (b) $L = 10$, and (c) $L = 100$: Diamonds show the PIMC results for $a/a_z = 0$, squares those for $a/a_z = 0.004\,33$, and triangles those for $a/a_z = 0.0433$ [24]; dotted lines show $(N_s/N)_{\hat{z}}$ for $a = 0$ calculated in the grand canonical ensemble. Solid lines show $(N_s/N)_{\hat{z}}$ given by Eq. (2). Dashed-dotted lines show N_0/N and dot-dot-dot-dashed lines the fraction N_{1D}/N. The inset of panel (a) shows $(N_s/N)_{\hat{x}}$ for $N = 27$ and $T/T_c = 0.2$ for three different interaction strengths (using the same symbols as in the main figure) as a function of L.

We now turn to the calculation of the superfluid fraction $(N_s/N)_{\hat{n}}$ with respect to the axis $\hat{n}$. For the noninteracting gas, the superfluid fraction with respect to, e.g., the z axis can be calculated from the thermal expectation values of x^2 and y^2 [19]. To this aim, we consider a trapping geometry with $\omega_y = \omega_x + \Delta\omega$ in the limit $\Delta\omega \to 0$ [see Eq. (7) in Ref. [19]]. Dotted lines in Fig. 3 show the resulting superfluid fraction $(N_s/N)_{\hat{z}}$, calculated in the grand canonical ensemble, for (a) $L = 1$, (b) $L = 10$, and (c) $L = 100$ as a function of T/T_c for $N = 27$ noninteracting bosons.

Within the PIMC formulation, the superfluid fraction $(N_s/N)_{\hat{n}}$ can be calculated from the square of the projected area $A_{\hat{n}}$ [11], where $A_{\hat{n}} = \vec{A} \cdot \hat{n}$ and $\vec{A}$ denotes the area enclosed by the imaginary time paths [9]. Symbols in Fig. 3 show the superfluid fraction $(N_s/N)_{\hat{z}}$ calculated using the PIMC method for three different aspect ratios L; diamonds show our results for $a = 0$, squares those for $a = 0.004\,33a_z$, and triangles those for $a = 0.0433a_z$. For $a = 0$, the PIMC results for $(N_s/N)_{\hat{z}}$ (diamonds), calculated in the canonical ensemble, agree well with those calculated in the grand canonical ensemble (dotted lines). The superfluid fraction $(N_s/N)_{\hat{z}}$ is essentially one at small scaled temperatures and decreases gradually with increasing T/T_c. For $L = 1$, $(N_s/N)_{\hat{z}}$ is about 0.05 for $T/T_c = 1$. For the larger aspect ratios [see Figs. 3(b) and 3(c)], in contrast, $(N_s/N)_{\hat{z}}$ is significantly larger at the transition temperature (about 0.2 for $L = 10$ and about 0.65 for $L = 100$). When plotted, as done here, as a function of T/T_c, the superfluid fraction $(N_s/N)_{\hat{z}}$ shows a very weak, if any, dependence on the interaction strength for all aspect ratios.

The spherically symmetric system with $L = 1$ has no preferred symmetry axis, implying $(N_s/N)_{\hat{z}} = (N_s/N)_{\hat{x}}$. For $L > 1$, however, the superfluid fraction $(N_s/N)_{\hat{x}}$ is distinctly different from $(N_s/N)_{\hat{z}}$. Geometric arguments imply that $(N_s/N)_{\hat{x}}$ approaches zero when the system reaches the quasi-1D regime. When exposed to a rotation about $\hat{x}$, the atoms move with the external trap, thus implying $\Theta_{\hat{x}}^{\mathrm{rig}} = \Theta_{\hat{x}}$. The inset in Fig. 3(a) shows the superfluid fraction $(N_s/N)_{\hat{x}}$ for $N = 27$ and $T/T_c = 0.2$ for three different scattering lengths (using the same symbols as in the main figure) as a function of the aspect ratio L. It is evident that $(N_s/N)_{\hat{x}}$ decreases rapidly with increasing L.

To connect with earlier work, we consider an analytical expression for the superfluid fraction $(N_s/N)_{\hat{z}}$, which has been derived using the semiclassical approximation for the noninteracting gas [19]. For a trap geometry with $\omega_y \approx \omega_x$ and $\omega_z = \omega_x/L$, we generalize the treatment by Stringari [19] to account for rotations about $\hat{n} = \hat{x}$. To additionally improve the accuracy for small N, we use the T_c that accounts for finite-size effects (see above),

$$(N_s/N)_{\hat{n}} = \frac{A[1-(T/T_c)^3]}{1-(\frac{T}{T_c})^3 + B\frac{1.80079}{L}(\frac{T}{T_c})^4 \frac{k_B T_c}{\hbar\omega_z}}. \quad (2)$$

Here A and B denote constants depending on the geometry of the trap; $A = B = 1$ for $\hat{n} = \hat{z}$, and $A = 1 - [(1-L)/(1+L)]^2$ and $B = (L^2+1)/(L+1)$ for $\hat{n} = \hat{x}$.

Solid lines in Fig. 3 show the resulting approximate superfluid fractions $(N_s/N)_{\hat{z}}$ (main figure) and $(N_s/N)_{\hat{x}}$ [inset in Fig. 3(a)]. The agreement between Eq. (2) and our numerical results for $L = 1$ is good. For $L = 100$, however, Eq. (2) describes the superfluid fraction at best qualitatively.

Since we expect the dependence of the condensate fraction N_0/N on the interaction strength to be small for the systems considered here, dashed-dotted lines in Fig. 3 show N_0/N calculated in the grand canonical ensemble for the noninteracting gas (N_0/N is defined as the occupation probability of the lowest oscillator state). For $L = 1$, the condensate fraction roughly agrees with the superfluid fraction. For $L = 100$, in contrast, N_0/N drops to zero at much lower temperatures than $(N_s/N)_{\hat{z}}$. This shows that the condensate fraction and the superfluid fraction are distinctly different quantities for highly elongated systems. For comparison, dot-dot-dot-dashed lines show the fraction of atoms N_{1D}/N in the lowest transverse mode, where $N_{1D} = \sum_k N_{00k}$ and N_{ijk}/N denotes the fraction of atoms in the state with i quanta in the x, j quanta in the y, and k quanta in the z directions. For the highly elongated gas with $L = 100$, the fraction of atoms N_{1D}/N is larger than the superfluid fraction $(N_s/N)_{\hat{z}}$ but shows a similar overall behavior.

Our calculations indicate that the superfluid fraction N_s/N and the condensate fraction N_0/N for $L = 1$ and $N = 27$ deviate at finite temperature even for the noninteracting gas [see Fig. 3(a)]. These deviations are somewhat enhanced for noninteracting gases with larger N, i.e., $N = 100$ and 1000 (not shown), implying that the deviations for $N = 27$ and $L = 1$ are not due to finite-size effects; N_s/N and N_0/N are distinctly different quantities at finite T, even for spherically symmetric noninteracting Bose gases. For highly elongated noninteracting Bose gases with up to $N = 1000$ (and constant L/N), we find that the ratio between N_s/N and N_{1D}/N at a given scaled temperature T/T_c remains roughly constant. We conclude that further systematic N-dependent investigations of the superfluid behavior of *noninteracting* and *interacting* Bose and Fermi gases with varying effective dimensionality are called for.

In summary, this Letter determines the quantum mechanical moment of inertia of small Bose gases under varying confinement over a wide temperature range. This quantity has played a key role in the study of finite-size bosonic helium droplets over the past 10 years or so [20]. Measurements of the quantum mechanical moment of inertia of an impurity embedded inside such a droplet have, e.g., shown unambigiously that bosonic helium clusters with as few as about 60 atoms are superfluid [21]. This paper shows that the effects of superfluidity are altered as the effective dimensionality of the trapped gas changes from 3D to 1D. The superfluid fraction $(N_s/N)_{\hat{z}}$ is enhanced as the dimensionality is reduced. In the quasi-1D regime, the superfluid response is distinctly different from the condensate fraction N_0/N and very roughly follows the fraction N_{1D}/N of atoms in the lowest transverse mode. Our predictions could be verified by extending experiments on rotating Bose gases [5] to optical lattices. Alternatively, spectroscopic measurements on impurities embedded in condensates [22] of different geometry might provide signatures of superfluidity.

We gratefully acknowledge fruitful discussions with S. Giorgini and support by the NSF, Grant No. PHY-0331529.

[1] R. J. Donnelly, *Quantized Vortices in Helium II* (Cambridge University Press, Cambridge, England, 1995).
[2] N. J. van Druten and W. Ketterle, Phys. Rev. Lett. **79**, 549 (1997).
[3] W. Ketterle and N. J. van Druten, Phys. Rev. A **54**, 656 (1996).
[4] M. R. Matthews *et al.*, Phys. Rev. Lett. **83**, 2498 (1999).
[5] K. W. Madison, F. Chevy, W. Wohlleben, and J. Dalibard, Phys. Rev. Lett. **84**, 806 (2000).
[6] J. R. Abo-Shaeer, C. Raman, J. M. Vogels, and W. Ketterle, Science **292**, 476 (2001).
[7] M. W. Zwierlein *et al.*, Nature (London) **435**, 1047 (2005).
[8] G. Baym, in *Mathematical Methods in Solid State and Superfluid Theory*, edited by R. C. Clark and E. H. Derrick (Oliver and Boyd, Edinburgh, 1969).
[9] D. M. Ceperley, Rev. Mod. Phys. **67**, 279 (1995).
[10] S. R. de Groot, G. J. Hooyman, and A. Seldam, Proc. R. Soc. A **203**, 266 (1950).
[11] P. Sindzingre, M. L. Klein, and D. M. Ceperley, Phys. Rev. Lett. **63**, 1601 (1989).
[12] A. Bohr and B. R. Mottelson, *Nuclear Structure*, Nuclear Deformations (W. A. Benjamin, Reading, 1975), Vol. II.
[13] F. Gerbier *et al.*, Phys. Rev. Lett. **92**, 030405 (2004).
[14] S. Inouye *et al.*, Nature (London) **392**, 151 (1998).
[15] M. Greiner *et al.*, Phys. Rev. Lett. **87**, 160405 (2001).
[16] C. Herzog and M. Olshanii, Phys. Rev. A **55**, 3254 (1997).
[17] F. Dalfovo, S. Giorgini, L. P. Pitaevskii, and S. Stringari, Rev. Mod. Phys. **71**, 463 (1999).
[18] See, e.g., D. S. Petrov, D. M. Gangardt, and G. V. Shlyapnikov, J. Phys. IV (France) **116**, 5 (2005).
[19] S. Stringari, Phys. Rev. Lett. **76**, 1405 (1996).
[20] J. P. Toennies, A. V. Vilesov, and K. B. Whaley, Phys. Today **54**, No. 2, 31 (2001).
[21] S. Grebenev, J. P. Toennies, and A. F. Vilesov, Science **279**, 2083 (1998).
[22] A. P. Chikkatur *et al.*, Phys. Rev. Lett. **85**, 483 (2000).
[23] Expectation values calculated by the PIMC method have an error bar since the technique is stochastic in nature.
[24] The PIMC data for small T/T_c have the largest error bars, the largest of which is at most 4 times the symbol size.